VNU Journal of Science: Mathematics – Physics, Vol. 42, No. 2 (2026) 86-98

VNU Journal of Science: Mathematics - Physics

Journal homepage: https://js.vnu.edu.vn/MaP

Original Article

Temperature and Pressure Effect on the Structural Properties of W and W-Fe Alloys

Duong Dai Phuong*

Military College of Tank Armour Officer, Km6, Tam Duong, Phu Tho

Received 6th December 2025
Revised 31st March 2026; Accepted 28th April 2026

Abstract: In this study, the Statistical Moment Method (SMM) is applied to investigate the structural properties of the W-Fe alloy at temperatures up to 3000 K and pressures up to 20 GPa. Analytical expressions for the free energy are derived, along with explicit formulas for structural quantities such as lattice constants and volume, taking into account the effects of anharmonicity. The results obtained from the SMM show good agreement with existing theoretical calculations and experimental data. This method demonstrates strong potential for further extension to the study of elastic properties, thermodynamic quantities, and the melting temperature of the W–Fe alloy in future work.

Keywords: W metal, $W_{15}Fe_1$ alloy, $W_{14}Fe_2$ alloy, structural properties, thermodynamic properties, temperature, high pressure, statistical moment method.

1. Introduction

Tungsten (W) is a refractory metal distinguished by its exceptionally high melting point (3422 °C), high density (19.3 g/cm^3), great hardness, and excellent resistance to wear and radiation. Owing to this unique property profile, it is a critical material for extreme environments, including aerospace and defense applications. Most notably, its high melting temperature, good thermal conductivity, and low erosion rate have established tungsten as the leading candidate material for plasma-facing components in future fusion reactors [1]. This viability has been successfully demonstrated in operational devices, most prominently through its full-scale implementation as the first wall material in the ASDEX Upgrade tokamak [2]. However, tungsten also exhibits certain drawbacks, including brittleness, low ductility, and poor radiation resistance. Studies have shown that alloying W with elements such as Re, Ni, Cu, Cr, and Ti can significantly improve these limitations [3-8].

* Corresponding author.
E-mail address: dphuong221059@gmail.com

https//doi.org/10.25073/2588-1124/vnumap.5099

Among these, the W–Fe alloy system is of particular importance, as it not only serves to bond tungsten with the steel substrate in reactors but also finds extensive applications in industry and defense [9]. The combination of W and Fe produces alloys that inherit high hardness, heat resistance, and wear resistance from W, while gaining improved ductility and machinability from Fe. However, the significant differences in melting point, density, crystal structure, and atomic size between W and Fe make fabrication challenging, often leading to segregation, phase separation, and reduced mechanical strength. In practice, Fe dissolves only a small amount in W, causing the alloy to generally exist as a two-phase system, with W particles dispersed in the Fe matrix, where internal stresses can easily develop and induce cracking. To overcome these issues, advanced fabrication techniques such as powder metallurgy, spark plasma sintering (SPS), hot isostatic pressing (HIP), and metal 3D printing have been employed to improve microstructural uniformity and stability. Consequently, W-Fe alloys exhibit great potential for applications in both defense and civilian industries, including armor-piercing projectiles, radiation shields, rocket nozzles, high-temperature electrodes, and wear-resistant components.

In recent years, the demand for materials capable of withstanding high temperatures and pressures has been steadily increasing to meet the requirements of fields such as nuclear energy, aerospace, and defense industries. In this context, theoretical calculations and material simulations have emerged as efficient, time- and cost-effective tools that help shorten the design cycle of new materials. Techniques such as molecular dynamics (MD), density functional theory (DFT), and multiscale modeling have been widely employed to study the microstructure as well as the physical, electrical, optical, mechanical, and thermodynamic properties of materials [10-12]. However, these methods often require extensive computational resources and high-performance computing systems.

In this context, the Statistical Moment Method (SMM), a modern theoretical approach in quantum statistical physics, has been proposed as a viable alternative. First developed in 1988 by Prof. Dr. Sci. Nguyen Huu Tang and Prof. Dr. Vu Van Hung [13], this method enables the calculation of thermodynamic and elastic properties of materials through explicit analytical expressions, using a fourth-order expansion of the interatomic potential, without requiring extensive input data. The SMM has been successfully applied to various types of materials with different crystal structures, such as BCC, FCC, HCP, perovskite, fluorite, and complex alloys [13-18]. Notably, this method has proven particularly effective for studying strongly anharmonic systems, where temperature effects on material properties cannot be neglected [18].

Before presenting the computational theory, we review studies related to each constituent element in the W-Fe system. For tungsten (W), recent *ab initio* simulations [19] have constructed the phase diagram of W under pressures up to several thousand GPa, showing the stability of the BCC structure as well as the phase transition to DHCP under extreme conditions. These results highlight the special role of W in the design of materials capable of withstanding high temperatures and pressures. For iron (Fe), it is a common metal with a density of 7,87 g/cm^3, melting point of 1538 °C, high ductility, and strong magnetism. At ambient pressure, Fe exists in a BCC structure, but it transforms to FCC at temperatures above 912 °C and to HCP under high pressure. Experimental phase diagrams [20] indicate that Fe undergoes multiple structural phase transitions depending on temperature and pressure, clearly reflecting the flexibility of this elemental crystal lattice.

2. Theoretical Basis

2.1. W-Fe Alloy Model and Helmholtz Free Energy

Based on previously proposed models for W-Fe alloys [21], we established a computational model derived from this approach. In this model, Fe atomic positions are considered to substitute at two atoms on the first coordination shell and two atoms on the second coordination shell, hereafter referred to as W_1 and W_2 positions, respectively.

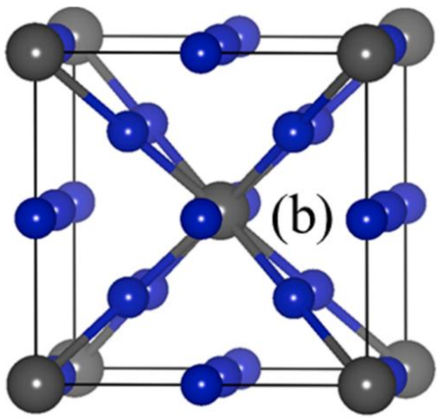

Figure 1. Model of the $W_{15}Fe_1$ alloy where the blue spheres are W and the gray-black spheres are Fe.

Consider the W-Fe alloy model with N atoms, which consists of N_{Fe} substituted Fe atoms, N_{W_1} W_1 atoms, N_{W_2} W_2 atoms, and $N_W = N - N_{W_1} - N_{W_2} - N_{Fe}$ W atoms. Let be the Helmholtz free energy corresponding to one atom A A = W, W_1, W_2 và Fe). The Helmholtz free energy [13] of the W-Fe alloy is equal to

$$\Psi_{WFe} = N_W\psi_W + N_{Fe}\psi_{Fe} + N_{W_1}\psi_{W_1} + N_{W_2}\psi_{W_2} - TS_c^{WFe}, \tag{1}$$

where T is the temperature and S_c^{WFe} is the configurational entropy of the W-Fe alloy. We have

$$\Psi_{WFe} = N\left(\frac{N_W}{N}\psi_W + \frac{N_{Fe}}{N}\psi_{Fe}\frac{N_{W_1}}{N}\psi_{W_1} + \frac{N_{W_2}}{N}\psi_{W_2}\right) - TS_c^{WFe} \tag{2}$$

where N_A is the number of atoms of type A and $c_A = \frac{N_A}{N}$ is the atomic concentration of A. Therefore,

$$\Psi_{WFe} = N\left(c_W\psi_W + c_{Fe}\psi_{Fe} + c_{W_1}\psi_{W_1} + c_{W_2}\psi_{W_2}\right) - TS_c^{WFe} = N\sum_A c_A\psi_A - TS_c. \tag{3}$$

In equation (3), $c_W = 1 - 8c_{Fe}$, $c_{W_1} = 4c_{Fe}$, $c_{W_2} = 3c_{Fe}$ corresponds to the W-Fe alloy, and the summation over A is taken over W, Fe, W_1, W_2. The Helmholtz free energy of an atom A is defined by [22]

$$\psi_A = \frac{\Psi_A}{N} = u_{0A} + \psi_{0A} + 3\left\{\frac{\theta^2}{k_A^2}\left[\gamma_{2A}Y_A^2 - \frac{2\gamma_{1A}}{3}\left(1 + \frac{Y_A}{2}\right)\right] + \right.$$
$$\left. + \frac{2\theta^3}{k_A^4}\left[\frac{4}{3}\gamma_{2A}^2Y_A\left(1 + \frac{Y_A}{2}\right) - 2\left(\gamma_{1A}^2 + 2\gamma_{1A}\gamma_{2A}\right)\left(1 + \frac{Y_A}{2}\right)\left(1 + Y_A\right)\right]\right\}, \tag{4}$$

With $Y_A \equiv x\coth x$ and $\psi_{0A} = \frac{\Psi_{0A}}{N} = 3\theta\left[x + \ln\left(1 - e^{-2x}\right)\right]$

In which u_{0A} is the binding energy of an A atom, ψ_{0A} is the free energy of a harmonic oscillator, $\theta = k_B T$, k_A, γ_{1A}, γ_{2A} are the crystal parameters for atom A $x = \frac{\hbar\omega_A}{2\theta} = \frac{\hbar}{2\theta}\sqrt{\frac{k_A}{m_A}}$, $\hbar = \frac{h}{2\pi}$, h is the Planck constant, ω_A is the vibrational frequency of atom A, and m_A is the mass of atom A.

When the concentration of Fe atoms is zero, then $\Psi_{WFe} = \Psi_W = N\psi_W$. In that case, u_0, k and γ_1, γ_2 are the binding energy and the lattice parameters of a W atom in the pure W metal [22].

$$u_0 \equiv \frac{1}{2}\sum_i \varphi_{i0},\ k \equiv \frac{1}{2}\sum_i \left(\frac{\partial^2 \varphi_{i0}}{\partial u_{i\beta}^2}\right)_{eq} = m\omega^2,$$

$$\gamma_1 \equiv \frac{1}{48}\sum_i \left(\frac{\partial^4 \varphi_{i0}}{\partial u_{i\beta}^4}\right)_{eq},\ \gamma_2 \equiv \frac{6}{48}\sum_i \left(\frac{\partial^4 \varphi_{i0}}{\partial u_{i\alpha}^2 \partial u_{i\beta}^2}\right)_{eq}. \tag{5}$$

In which $u_{i\beta}(\beta = x, y, z)$ is the displacement of the i-th particle from its equilibrium position in the direction β, and φ_{i0} is the interaction potential between the 0-th particle and the i-th particle. The free energy of the metal at temperature T can be calculated if u_0, k, γ_1 and γ_2 are known at a temperature T_0 (such as T_0 = 0 K).

2.2. Binding Energy and Alloy Parameters

Consider pure tungsten W with a BCC structure, the binding energy u_{0W} and the crystal parameters k_W, γ_{1W}, γ_{2W}, γ_W of the W atom in the 5-coordination sphere approximation centered at the atom's position with radii r_{1W} and $r_{2W} = \frac{2r_{1W}}{\sqrt{3}}; r_{3W} = \frac{\sqrt{8}r_{1W}}{\sqrt{3}}; r_{4W} = \frac{\sqrt{11}r_{1W}}{\sqrt{3}}; r_{5W} = \frac{\sqrt{12}r_{1W}}{\sqrt{3}}$, are expressed as

$$u_{0W} = \frac{1}{2}\sum_{i=1}^{n_i}\varphi_W(r_{iW}) = 4\varphi_W(r_{1W}) + 3\varphi_W(r_{2W}) + 6\varphi_W(r_{3W}) + 12\varphi_W(r_{4W}) + 4\varphi_W(r_{5W}), \tag{6}$$

$$\begin{aligned} k_W &= \frac{1}{2}\sum_i^{n_i}\left(\frac{\partial^2 \varphi_W}{\partial u_{i\beta}^2}\right)_{eq} = \frac{4}{3}\frac{d^2\varphi_W(r_{1W})}{dr_{1W}^2} + \frac{8}{3r_{1W}}\frac{d\varphi_W(r_{1W})}{dr_{1W}} + \frac{d^2\varphi_W(r_{2W})}{dr_{2W}^2} \\ &+ \frac{2}{r_{2W}}\frac{d\varphi_W(r_{2W})}{dr_{2W}} + \frac{8}{3}\frac{d^2\varphi_W(r_{3W})}{dr_{3W}^2} + \frac{1}{3r_{3W}}\frac{d\varphi_W(r_{3W})}{dr_{3W}}, \end{aligned} \tag{7}$$

$$\gamma_{1A} = \frac{1}{48}\sum_i^{n_i}\left(\frac{\partial^4 \varphi_{AA}}{\partial u_{i\beta}^4}\right)_{eq} = \frac{1}{54}\frac{d^4\varphi_W(r_{1W})}{dr_{1W}^4} + \frac{2}{9r_{1W}}\frac{d^3\varphi_W(r_{1W})}{dr_{1W}^3} - \frac{2}{9r_{1W}^2}\frac{d^2\varphi_W(r_{1W})}{dr_{1W}^2} + \frac{2}{9r_{1W}^3}\frac{d\varphi_W(r_{1W})}{dr_{1W}} \tag{8}$$

$$+\frac{1}{24}\frac{d^4\varphi_W(r_{2W})}{dr_{2W}^4}+\frac{1}{4r_{2W}^2}\frac{d^2\varphi_W(r_{2W})}{dr_{2W}^2}-\frac{1}{4r_{2W}^3}\frac{d\varphi_W(r_{2W})}{dr_{2W}}$$
$$+\frac{8}{27}\frac{d^4\varphi_W(r_{3W})}{dr_{3W}^4}-\frac{4}{9r_{3W}}\frac{d^3\varphi_W(r_{3W})}{dr_{3W}^3}+\frac{43}{36r_{3W}^2}\frac{d^2\varphi_W(r_{3W})}{dr_{3W}^2}-\frac{43}{36r_{3W}^3}\frac{d\varphi_W(r_{3W})}{dr_{3W}},$$

$$\gamma_{2A}=\frac{6}{48}\sum_i^{n_i}\left(\frac{\partial^4\varphi_{AA}}{\partial u_{i\alpha}^2\partial u_{i\beta}^2}\right)_{eq}=\frac{1}{9}\frac{d^4\varphi_W(r_{1W})}{dr_{1W}^4}+\frac{2}{3r_{1W}^2}\frac{d^2\varphi_W(r_{1W})}{dr_{1W}^2}-\frac{2}{3r_{1W}^3}\frac{d\varphi_W(r_{1W})}{dr_{1W}}$$
$$+\frac{1}{2r_{2W}}\frac{d^3\varphi_W(r_{2W})}{dr_{2W}^4}-\frac{3}{4r_{2W}^2}\frac{d^2\varphi_W(r_{2W})}{dr_{2W}^2}+\frac{3}{4r_{2W}^3}\frac{d\varphi_W(r_{2W})}{dr_{2W}} \tag{9}$$
$$+\frac{8}{9}\frac{d^4\varphi_W(r_{3W})}{dr_{3W}^4}-\frac{4}{3r_{3W}}\frac{d^3\varphi_W(r_{3W})}{dr_{3W}^3}+\frac{17}{6r_{3W}^2}\frac{d^2\varphi_W(r_{3W})}{dr_{3W}^2}-\frac{17}{6r_{3W}^3}\frac{d\varphi_W(r_{3W})}{dr_{3W}}.$$

In the formulas from (6) to (9), φ_W is the pairwise interaction potential between two atoms of the metal, n_i is the number of atoms on the i-th coordination shell, and $u_{i\alpha}$, $u_{i\beta}$ are the displacement of the i-th atom in the α, β direction, with $\alpha, \beta = x, y, z, \alpha \neq \beta$.

Considering the W-Fe alloy model with a BCC structure, the binding energy u_{0Fe} and the crystal parameters k_{Fe}, γ_{1Fe}, γ_{2Fe}, γ_{Fe} of the substituting Fe atom in the 5-coordination sphere approximation center at the Fe atom's position and the radii being r_{1WFe} and $r_{2Fe}=\frac{2r_{1Fe}}{\sqrt{3}};r_{3Fe}=\frac{\sqrt{8}r_{1Fe}}{\sqrt{3}};r_{4Fe}=\frac{\sqrt{11}r_{1Fe}}{\sqrt{3}};r_{5Fe}=\frac{\sqrt{12}r_{1Fe}}{\sqrt{3}}$, take the form

$$u_{0Fe}=\frac{1}{2}\sum_{i=1}^{n_i}\varphi_{\mathrm{WFe}}(r_{iFe})=4\varphi_{\mathrm{WFe}}(r_{1Fe})+3\varphi_{\mathrm{WFe}}(r_{2Fe})+6\varphi_{\mathrm{WFe}}(r_{3Fe})+12\varphi_{\mathrm{WFe}}(r_{4Fe})+4\varphi_{\mathrm{WFe}}(r_{5Fe}), \tag{10}$$

$$k_{Fe}=\frac{1}{2}\sum_i^{n_i}\left(\frac{\partial^2\varphi_{\mathrm{WFe}}}{\partial u_{i\beta}^2}\right)_{eq}=\frac{4}{3}\frac{d^2\varphi_{WFe}(r_{1Fe})}{dr_{1Fe}^2}+\frac{8}{3r_{1Fe}}\frac{d\varphi_{WFe}(r_{1Fe})}{dr_{1Fe}}+\frac{d^2\varphi_{WFe}(r_{2Fe})}{dr_{2Fe}^2}$$
$$+\frac{2}{r_{2Fe}}\frac{d\varphi_{WFe}(r_{2Fe})}{dr_{2Fe}}+\frac{8}{3}\frac{d^2\varphi_{WFe}(r_{3Fe})}{dr_{3Fe}^2}+\frac{1}{3r_{3Fe}}\frac{d\varphi_{WFe}(r_{3Fe})}{dr_{3Fe}}, \tag{11}$$

$$\gamma_{Fe}=4(\gamma_{1Fe}+\gamma_{2Fe}), \tag{12}$$

$$\gamma_{1Fe}=\frac{1}{48}\sum_i^{n_i}\left(\frac{\partial^4\varphi_{\mathrm{WFe}}}{\partial u_{i\beta}^4}\right)_{eq}=\frac{1}{54}\frac{d^4\varphi_{WFe}(r_{1Fe})}{dr_{1Fe}^4}+\frac{2}{9r_{1Fe}}\frac{d^3\varphi_{WFe}(r_{1Fe})}{dr_{1Fe}^3}-\frac{2}{9r_{1Fe}^2}\frac{d^2\varphi_{WFe}(r_{1Fe})}{dr_{1Fe}^2}+\frac{2}{9r_{1Fe}^3}\frac{d\varphi_{WFe}(r_{1Fe})}{dr_{1Fe}}$$
$$+\frac{1}{24}\frac{d^4\varphi_{WFe}(r_{2Fe})}{dr_{2Fe}^4}+\frac{1}{4r_{2Fe}^2}\frac{d^2\varphi_{WFe}(r_{2Fe})}{dr_{2Fe}^2}-\frac{1}{4r_{2Fe}^3}\frac{d\varphi_{WFe}(r_{2Fe})}{dr_{2Fe}} \tag{13}$$
$$+\frac{8}{27}\frac{d^4\varphi_{WFe}(r_{3Fe})}{dr_{3Fe}^4}-\frac{4}{9r_{3Fe}}\frac{d^3\varphi_{WFe}(r_{3Fe})}{dr_{3Fe}^3}+\frac{43}{36r_{3Fe}^2}\frac{d^2\varphi_{WFe}(r_{3Fe})}{dr_{3Fe}^2}-\frac{43}{36r_{3Fe}^3}\frac{d\varphi_{WFe}(r_{3Fe})}{dr_{3Fe}},$$

$$\gamma_{2Fe} = \frac{6}{48}\sum_{i}^{n_i}\left(\frac{\partial^4 \varphi_{\mathrm{W}Fe}}{\partial u_{i\alpha}^2 \partial u_{i\beta}^2}\right)_{eq} = \frac{1}{9}\frac{d^4\varphi_{WFe}\left(r_{1Fe}\right)}{dr_{1Fe}^4} + \frac{2}{3r_{1Fe}^2}\frac{d^2\varphi_{WFe}\left(r_{1Fe}\right)}{dr_{1Fe}^2} - \frac{2}{3r_{1Fe}^3}\frac{d\varphi_{WFe}\left(r_{1Fe}\right)}{dr_{1Fe}}$$
$$+\frac{1}{2r_{2Fe}}\frac{d^3\varphi_{WFe}\left(r_{2Fe}\right)}{dr_{2Fe}^4} - \frac{3}{4r_{2Fe}^2}\frac{d^2\varphi_{WFe}\left(r_{2Fe}\right)}{dr_{2Fe}^2} + \frac{3}{4r_{2Fe}^3}\frac{d\varphi_{WFe}\left(r_{2Fe}\right)}{dr_{2Fe}}$$
$$+\frac{8}{9}\frac{d^4\varphi_{WFe}\left(r_{3Fe}\right)}{dr_{3Fe}^4} - \frac{4}{3r_{3Fe}}\frac{d^3\varphi_{WFe}\left(r_{3Fe}\right)}{dr_{3Fe}^3} + \frac{17}{6r_{3Fe}^2}\frac{d^2\varphi_{WFe}\left(r_{3Fe}\right)}{dr_{3Fe}^2} - \frac{17}{6r_{3Fe}^3}\frac{d\varphi_{WFe}\left(r_{3Fe}\right)}{dr_{3Fe}}, \tag{14}$$

The binding energy $u_{0\mathrm{W}_1}$ and the crystal parameters k_{W_1}, $\gamma_{1\mathrm{W}_1}$, $\gamma_{2\mathrm{W}_1}$, γ_{W_1} for the W_1 substitutional atom in the W-Fe model in the 4-coordination shell approximation are, respectively, r_{1W_1} and $r_{2W_1} = \frac{2r_{1W_1}}{\sqrt{3}}; r_{3W_1} = \frac{\sqrt{8}r_{1W_1}}{\sqrt{3}}; r_{4W_1} = \frac{\sqrt{11}r_{1W_1}}{\sqrt{3}}$ and have the form:

$$u_{0\mathrm{W}_1} = \frac{1}{2}\sum_{i=1}^{n_i}\varphi_{\mathrm{W}_1}(r_{i\mathrm{W}_1}) = \varphi_{\mathrm{W}_1\mathrm{Fe}}\left(r_{1W_1}\right) + 3\varphi_{\mathrm{W}}\left(r_{1W_1}\right) + 3\varphi_{\mathrm{W}}\left(r_{2W_1}\right) + 6\varphi_{\mathrm{W}}\left(r_{3W_1}\right) + 12\varphi_{\mathrm{W}}\left(r_{4W_1}\right), \tag{15}$$

$$k_{\mathrm{W}_1} = \frac{1}{2}\sum_{i}^{n_i}\left[\left(\frac{\partial^2\varphi_{\mathrm{W}_1}}{\partial u_{i\beta}^2}\right)_{eq}\right] = \frac{2}{6}\frac{d^2\varphi_{WFe}\left(r_{1W_1}\right)}{dr_{1W_1}^2} - \frac{1}{3r_{1W_1}}\frac{d\varphi_W\left(r_{1W_1}\right)}{dr_{1W_1}} + \frac{4}{6}\frac{d^2\varphi_{WCr}\left(r_{1W_1}\right)}{dr_{1W_1}^2} + \frac{3}{r_{1W_1}}\frac{d\varphi_W\left(r_{1W_1}\right)}{dr_{1W_1}}$$
$$+2\frac{d^2\varphi_W\left(r_{2W_1}\right)}{dr_{2W_1}^2} + \frac{4}{r_{2W_1}}\frac{d\varphi_W\left(r_{2W_1}\right)}{dr_{2W_1}} + \frac{16}{3}\frac{d^2\varphi_W\left(r_{3W_1}\right)}{dr_{3W_1}^2} + \frac{2}{3r_{3W_1}}\frac{d\varphi_W\left(r_{3W_1}\right)}{dr_{3W_1}}, \tag{16}$$

$$\gamma_{\mathrm{W}_1} = 4\left(\gamma_{1\mathrm{W}_1} + \gamma_{2\mathrm{W}_1}\right), \tag{17}$$

$$\gamma_{1\mathrm{W}_1} = \frac{1}{48}\sum_{i}^{n_i}\left[\left(\frac{\partial^4\varphi_{\mathrm{W}_1}}{\partial u_{i\beta}^4}\right)_{eq}\right] = \frac{2}{432}\frac{d^4\varphi_{WFe}\left(r_{1\mathrm{W}_1}\right)}{dr_{1\mathrm{W}_1}^4} + \frac{2}{36r_{1\mathrm{W}_1}}\frac{d^3\varphi_{WFe}\left(r_{1\mathrm{W}_1}\right)}{dr_{1\mathrm{W}_1}^3}$$
$$-\frac{2}{36r_{1\mathrm{W}_1}^2}\frac{d^2\varphi_{WFe}\left(r_{1\mathrm{W}_1}\right)}{dr_{1\mathrm{W}_1}^2} + \frac{2}{36r_{1\mathrm{W}_1}^3}\frac{d\varphi_{WFe}\left(r_{1\mathrm{W}_1}\right)}{dr_{1\mathrm{W}_1}} +$$
$$+\frac{6}{432}\frac{d^4\varphi_W\left(r_{1\mathrm{W}_1}\right)}{dr_{1\mathrm{W}_1}^4} + \frac{6}{36r_{1\mathrm{W}_1}}\frac{d^3\varphi_W\left(r_{1\mathrm{W}_1}\right)}{dr_{1\mathrm{W}_1}^3} - \frac{6}{36r_{1\mathrm{W}_1}^2}\frac{d^2\varphi_W\left(r_{1\mathrm{W}_1}\right)}{dr_{1\mathrm{W}_1}^2} + \frac{6}{36r_{1\mathrm{W}_1}^3}\frac{d\varphi_W\left(r_{1\mathrm{W}_1}\right)}{dr_{1\mathrm{W}_1}}$$
$$+\frac{1}{24}\frac{d^4\varphi_W\left(r_{2\mathrm{W}_1}\right)}{dr_{2\mathrm{W}_1}^4} + \frac{1}{4r_{2\mathrm{W}_1}^2}\frac{d^2\varphi_W\left(r_{2\mathrm{W}_1}\right)}{dr_{2\mathrm{W}_1}^2} - \frac{1}{4r_{2\mathrm{W}_1}^3}\frac{d\varphi_W\left(r_{2\mathrm{W}_1}\right)}{dr_{2\mathrm{W}_1}}$$
$$+\frac{8}{27}\frac{d^4\varphi_W\left(r_{3\mathrm{W}_1}\right)}{dr_{3\mathrm{W}_1}^4} - \frac{4}{9r_{3\mathrm{W}_1}}\frac{d^3\varphi_W\left(r_{3\mathrm{W}_1}\right)}{dr_{3\mathrm{W}_1}^3} + \frac{43}{36r_{3\mathrm{W}_1}^2}\frac{d^2\varphi_W\left(r_{3\mathrm{W}_1}\right)}{dr_{3\mathrm{W}_1}^2} - \frac{43}{36r_{3\mathrm{W}_1}^3}\frac{d\varphi_W\left(r_{3\mathrm{W}_1}\right)}{dr_{3\mathrm{W}_1}}, \tag{18}$$

$$\gamma_{2W_1} = \frac{6}{48}\sum_i^{n_i}\left[\left(\frac{\partial^4\varphi_{W_1}}{\partial u_{i\alpha}^2\partial u_{i\beta}^2}\right)_{eq}\right] = \frac{2}{36}\frac{d^4\varphi_{WFe}\left(r_{1W_1}\right)}{dr_{1W_1}^4} + \frac{2}{48r_{1W_1}^2}\frac{d^2\varphi_{WFe}\left(r_{1W_1}\right)}{dr_{1W_1}^2} - \frac{2}{48r_{1W_1}^3}\frac{d\varphi_{WFe}\left(r_{1W_1}\right)}{dr_{1W_1}}$$
$$+\frac{2}{12}\frac{d^4\varphi_W\left(r_{1W_1}\right)}{dr_{1W_1}^4} + \frac{30}{48r_{1W_1}^2}\frac{d^2\varphi_W\left(r_{1W_1}\right)}{dr_{1W_1}^2} - \frac{30}{48r_{1W_1}^3}\frac{d\varphi_W\left(r_{1W_1}\right)}{dr_{1W_1}}$$
$$+\frac{1}{2r_{2Fe}}\frac{d^3\varphi_W\left(r_{2W_1}\right)}{dr_{2W_1}^4} - \frac{3}{4r_{2W_1}^2}\frac{d^2\varphi_W\left(r_{2W_1}\right)}{dr_{2W_1}^2} + \frac{3}{4r_{2W_1}^3}\frac{d\varphi_W\left(r_{2W_1}\right)}{dr_{2W_1}} \tag{19}$$
$$+\frac{8}{9}\frac{d^4\varphi_W\left(r_{3W_1}\right)}{dr_{3W_1}^4} - \frac{4}{3r_{3W_1}}\frac{d^3\varphi_W\left(r_{3W_1}\right)}{dr_{3W_1}^3} + \frac{17}{6r_{3W_1}^2}\frac{d^2\varphi_W\left(r_{3W_1}\right)}{dr_{3W_1}^2} - \frac{17}{6r_{3W_1}^3}\frac{d\varphi_W\left(r_{3W_1}\right)}{dr_{3W_1}},$$

The binding energy u_{0W_2} and the crystal parameters k_{W_2}, γ_{1W_2}, γ_{2W_2}, γ_{W_2} for the W_2 substitutional atom in the W-Fe model in the 4-coordination shell approximation are, respectively, r_{1W_2} and $r_{2W_2} = \frac{2r_{1W_2}}{\sqrt{3}}; r_{3W_2} = \frac{\sqrt{8}r_{1W_2}}{\sqrt{3}}; r_{4W_2} = \frac{\sqrt{11}r_{1W_2}}{\sqrt{3}}$ and have the form:

$$u_{0W_2} = \frac{1}{2}\sum_{i=1}^{n_i}\varphi_{W_2}(r_{iW_2}) = 4\varphi_W\left(r_{1W_2}\right) + 1\varphi_{WFe}\left(r_{2W_2}\right) + 2\varphi_W\left(r_{2W_2}\right) + 6\varphi_W\left(r_{3W_2}\right) + 12\varphi_W\left(r_{4W_2}\right), \tag{20}$$

$$k_{W_2} = \frac{1}{2}\sum_i^{n_i}\left[\left(\frac{\partial^2\varphi_{W_2}}{\partial u_{i\beta}^2}\right)_{eq}\right] = \frac{4}{3}\frac{d^2\varphi_{WFe}\left(r_{1W_2}\right)}{dr_{1W_2}^2} + \frac{8}{3r_{1W_2}}\frac{d\varphi_W\left(r_{1W_2}\right)}{dr_{1W_2}} + \frac{1}{2}\frac{d^2\varphi_{WFe}\left(r_{2W_2}\right)}{dr_{2W_2}^2}$$
$$+\frac{1}{2}\frac{d^2\varphi_W\left(r_{2W_2}\right)}{dr_{2W_2}^2} + \frac{2}{r_{2W_2}}\frac{d\varphi_W\left(r_{2W_2}\right)}{dr_{2W_2}} + \frac{16}{3}\frac{d^2\varphi_W\left(r_{3W_2}\right)}{dr_{3W_2}^2} + \frac{2}{3r_{3W_2}}\frac{d\varphi_W\left(r_{3W_2}\right)}{dr_{3W_2}}, \tag{21}$$

$$\gamma_{W_2} = 4\left(\gamma_{1W_2} + \gamma_{2W_2}\right), \tag{22}$$

$$\gamma_{1W_2} = \frac{1}{48}\sum_i^{n_i}\left[\left(\frac{\partial^4\varphi_{W_2}}{\partial u_{i\beta}^4}\right)_{eq}\right] = \frac{1}{54}\frac{d^4\varphi_W\left(r_{1W_2}\right)}{dr_{1W_2}^4} + \frac{2}{9r_{1W_2}}\frac{d^3\varphi_W\left(r_{1W_2}\right)}{dr_{1W_2}^3} - \frac{2}{9r_{1W_2}^2}\frac{d^2\varphi_W\left(r_{1W_2}\right)}{dr_{1W_2}^2} + \frac{2}{9r_{1W_2}^3}\frac{d\varphi_W\left(r_{1W_2}\right)}{dr_{1W_2}}$$
$$+\frac{1}{48}\frac{d^4\varphi_W\left(r_{2W_2}\right)}{dr_{2W_2}^4} + \frac{3}{32r_{2W_2}}\frac{d^3\varphi_W\left(r_{2W_2}\right)}{dr_{2W_2}^3} + \frac{1}{4r_{2W_2}^2}\frac{d^2\varphi_W\left(r_{2W_2}\right)}{dr_{2W_2}^2} - \frac{1}{4r_{2W_2}^3}\frac{d\varphi_W\left(r_{2W_2}\right)}{dr_{2W_2}}$$
$$+\frac{1}{48}\frac{d^4\varphi_{WFe}\left(r_{2W_2}\right)}{dr_{2W_2}^4} - \frac{3}{32r_{2W_2}}\frac{d^3\varphi_{WFe}\left(r_{2W_2}\right)}{dr_{2W_2}^3} + \frac{8}{27}\frac{d^4\varphi_W\left(r_{3W_2}\right)}{dr_{3W_2}^4} - \frac{4}{9r_{3W_2}}\frac{d^3\varphi_W\left(r_{3W_2}\right)}{dr_{3W_2}^3} \tag{23}$$
$$+\frac{43}{36r_{3W_2}^2}\frac{d^2\varphi_W\left(r_{3W_2}\right)}{dr_{3W_2}^2} - \frac{43}{36r_{3W_2}^3}\frac{d\varphi_W\left(r_{3W_2}\right)}{dr_{3W_2}},$$

$$\gamma_{2W_2} = \frac{6}{48}\sum_i^{n_i}\left[\left(\frac{\partial^4\varphi_{W_2}}{\partial u_{i\alpha}^2\partial u_{i\beta}^2}\right)_{eq}\right] = \frac{1}{9}\frac{d^4\varphi_W\left(r_{1W_2}\right)}{dr_{1W_2}^4} + \frac{2}{3r_{1W_2}^2}\frac{d^2\varphi_W\left(r_{1W_2}\right)}{dr_{1W_2}^2} - \frac{2}{3r_{1W_2}^3}\frac{d\varphi_W\left(r_{1W_2}\right)}{dr_{1W_2}}$$
$$+\frac{3}{8r_{2W_2}}\frac{d^3\varphi_W\left(r_{2W_2}\right)}{dr_{2W_2}^4} - \frac{7}{16r_{2W_2}^2}\frac{d^2\varphi_W\left(r_{2W_2}\right)}{dr_{2W_2}^2} + \frac{7}{16r_{2W_2}^3}\frac{d\varphi_W\left(r_{2W_2}\right)}{dr_{2W_2}}$$
$$+\frac{1}{8}\frac{d^4\varphi_{WFe}\left(r_{2W_2}\right)}{dr_{2W_2}^4} - \frac{5}{16r_{2W_2}^2}\frac{d^2\varphi_{WFe}\left(r_{2W_2}\right)}{dr_{2W_2}^2} + \frac{5}{16r_{2W_2}^3}\frac{d\varphi_{WFe}\left(r_{2W_2}\right)}{dr_{2W_2}} \tag{24}$$
$$+\frac{8}{9}\frac{d^4\varphi_W\left(r_{3W_2}\right)}{dr_{3W_2}^4} - \frac{4}{3r_{3W_2}}\frac{d^3\varphi_W\left(r_{3W_2}\right)}{dr_{3W_2}^3} + \frac{17}{6r_{3W_2}^2}\frac{d^2\varphi_W\left(r_{3W_2}\right)}{dr_{3W_2}^2} - \frac{17}{6r_{3W_2}^3}\frac{d\varphi_W\left(r_{3W_2}\right)}{dr_{3W_2}},$$

2.3. Equation of State and Average Nearest-neighbor Distance Between Two Atoms in the W-Fe Alloy Model

The nearest-neighbor distance between two W atoms in pure W metal and the nearest-neighbor distance between atom A (A = W_1, W_2, Fe) and another atom at temperature T and pressure P in the W-Fe alloy model with a cubic structure can be determined by the following equation of state [22]:

$$Pv_A + r_{1A}\left(\frac{1}{6}\frac{\partial u_{0A}}{\partial r_{1A}} + \theta Y_A\frac{1}{2k_A}\frac{\partial k_A}{\partial r_{1A}}\right) = 0, \tag{25}$$

in which $v_A = \frac{4r_{1A}^3}{3\sqrt{3}}$. When $T = 0$ K and pressure P, (25) becomes [22]

$$Pv_A + r_{1A}\left(\frac{1}{6}\frac{\partial u_{0A}}{\partial r_{1A}} + \frac{\hbar\omega_{0A}}{4k_A}\frac{\partial k_A}{\partial r_{1A}}\right) = 0. \tag{26}$$

When the interatomic potential between two W and Fe atoms is known, equation (25) allows for the determination of the nearest neighbor distance $r_{1A}(P,0)$ $(A = W, W_1, W_2, Fe)$ and the crystal parameters $k_A(P,0), \gamma_{1A}(P,0), \gamma_{2A}(P,0), \gamma_A(P,0)$ at pressure P and 0 K. From there, we can determine the displacement $y_A(P,T) = \sqrt{\frac{2\gamma_A\theta^2}{3(k_A)^3}}\Delta_A$, of atom A at pressure P and temperature T from its equilibrium position by solving the force balance equation using the iterative method [22]. Subsequently, the average nearest neighbor distance between two W atoms in the W-Fe alloy model with a cubic structure at pressure P and temperature T is determined by:

$$\overline{r_1(P,T)} = \overline{r_1(P,0)} + \overline{y(P,T)},\ \ \overline{r_1(P,0)} = \left(1 - c_{Fe}\right)r_{1W}(P,0) + c_{Fe}r_{1Fe}(P,0), \tag{27}$$

$$\overline{y(P,T)} = c_W y_W(P,T) + c_{Fe}y_{Fe}(P,T) + c_{W_1}y_{W_1}(P,T) + c_{W_2}y_{W_2}(P,T), \tag{28}$$

in which: $c_W = 1 - 8c_{Fe}$, $c_{W_1} = 4c_{Fe}$ and $c_{W_2} = 3c_{Fe}$, $\overline{r_1(P,0)}$ are the average nearest neighbor distances between two A atoms in the W-Fe alloy model at pressure P and temperature 0 K, $\overline{y(P,T)}$ is the average displacement of the W atom from its equilibrium position at pressure *P* and temperature *T*, $r_{1\mathrm{W}}(P,0)$ is the nearest neighbor distance between two W atoms in pure W metal at pressure *P* and temperature 0 K, and $r_{1Fe}(P,0)$ is the nearest neighbor distance between two W atoms when the Fe substitutional site is chosen as the origin at pressure *P* and temperature 0 K.

2.4. Structural Properties of W-Fe Alloys

The lattice constant of the W-Fe alloy at pressure *P* and temperature *T* is determined by:

$$a = \frac{2}{\sqrt{3}}\left(\overline{r_1(P,T)} + \overline{y(P,T)}\right), \tag{29}$$

The molar volume of the W-Fe alloy is calculated by:

$$V = \frac{4}{3\sqrt{3}}\left(\overline{r_1(P,T)} + \overline{y(P,T)}\right)^3, \tag{30}$$

3. Numerical Results and Discussion

For crystals with Face-Centered Cubic (FCC) and Body-Centered Cubic (BCC) structures, the potential form we chose for investigation is the m-n interaction potential [23]:

$$\varphi_{\mathrm{ij}}(r) = \frac{D}{n-m}\left[m\left(\frac{r_0}{r_{\mathrm{ij}}}\right)^n - n\left(\frac{r_0}{r_{\mathrm{ij}}}\right)^m\right] \tag{31}$$

and we approximate the W-Fe interaction potential as given by:

$$\varphi_{W-Fe} \approx \frac{1}{2}\left(\varphi_{W-\mathrm{W}} + \varphi_{Fe-Fe}\right) \tag{32}$$

Table 1. Mie–Lennard-Jones potential parameters for tungsten (W) and iron (Fe)

	D/k_B (K)	m	n	$r_o(10^{-10}$m)
W – W [23]	25608.93	4.06	8.58	2.7365
Fe – Fe [23]	12576.70	3.58	8.26	2.4775

Here, D is the potential well depth, m and n are constants, r_{ij} is the distance between atoms i and j, and r_0 is the equilibrium value of r_{ij}.

Figure 2: Graph showing the dependence of the lattice constant on temperature for pure W (W Pure), $W_{15}Fe_1$ alloy, and $W_{14}Fe_2$ alloy. In the temperature range from 0 K to 3000 K, all three curves exhibit an upward trend, indicating that the lattice constant of W metal and the W-Fe alloys increases with temperature- a common characteristic of metals. Pure W has the largest lattice constant and the steepest slope, demonstrating that this material expands strongly with temperature. When iron atoms are introduced, as in $W_{15}Fe_1$ (red line), the expansion capability is slightly reduced; and in $W_{14}Fe_2$ (blue line), with a higher concentration of Fe atoms, the expansion is even lower, and the lattice constant also decreases. This is explained by the influence of Fe atoms, which are smaller than W and form stronger bonds, making the crystal lattice more stable and more resistant to expansion. Thus, Fe doping helps

tune the expansion characteristics of Tungsten, opening up applications in functional materials or high-temperature thermal engineering. Furthermore, at high temperatures, from 2500K to 3000K, the slope of the graph is steep, and the lattice constant increases sharply. This signifies the strong contribution of the anharmonic effect to the lattice vibrations.

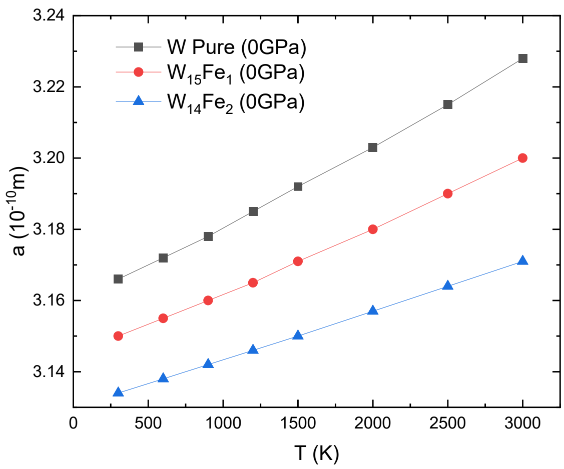

Figure 2. Temperature dependence of the lattice constant for W and W–Fe alloys.

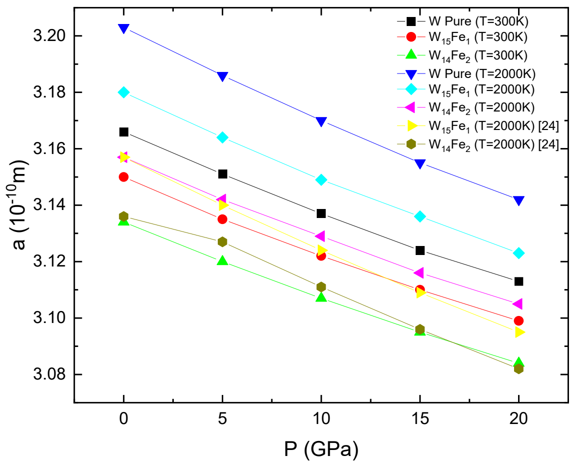

Figure 3. Pressure dependence of the lattice constant for W and W–Fe alloys at 300 K and 2000 K.

Figure 3: Diagram describing the change in lattice constant as a function of pressure from 0 GPa to 20GPa at temperatures of 300 K and 2000 K for W and W-Fe alloys. All represented curves show a downward, decreasing trend, indicating that as pressure increases, the size of the unit cell decreases - a commonly observed crystal compression phenomenon. Pure W has the highest initial *a* value ($\sim 3.20\times 10^{-10}$ m) but is compressed more significantly compared to the doped samples. In contrast, $W_{15}Fe_1$ and especially $W_{14}Fe_2$ have a smaller lattice constant and a less steep reduction in slope, demonstrating a denser crystal lattice and better resistance to compression. This is attributed to the Fe atoms contributing to a more stable lattice structure under pressure. The results suggest that $W_{14}Fe_2$ is a potential material for applications requiring resistance to both high temperature and high pressure. The calculation results obtained by the SMM (Statistical Moment Method) for the W-Fe alloy regarding the pressure dependence of the lattice constant at 300K show good agreement when compared with calculations from reference [24].

Figure 4: Graph illustrating the change in atomic volume with temperature from 0K to 3000 K for W and W-Fe alloys, where both calculated and experimental data show an increasing trend with temperature - reflecting the characteristic thermal expansion phenomenon in metals. The pure W sample (W pure) exhibits the largest atomic volume ($\sim 32 \times 10^{-30}$ m^3 at 0K) and the steepest slope of increase, indicating a high degree of thermal expansion. The experimental data for W Pure [25] (light green line) is nearly coincident with the simulated results, confirming the reliability of the model. The two Fe alloy samples ($W_{15}Fe_1$ and $W_{14}Fe_2$) have a smaller initial volume because the smaller Fe atoms substitute the W positions, causing the crystal lattice to contract. Among them, $W_{14}Fe_2$, with a higher Fe content, has the lowest volume and the least expansion, demonstrating a more stable structure as the temperature increases. Thus, alloying Fe into W reduces the atomic volume and limits expansion, which can be beneficial for applications under high-temperature conditions requiring geometric stability.

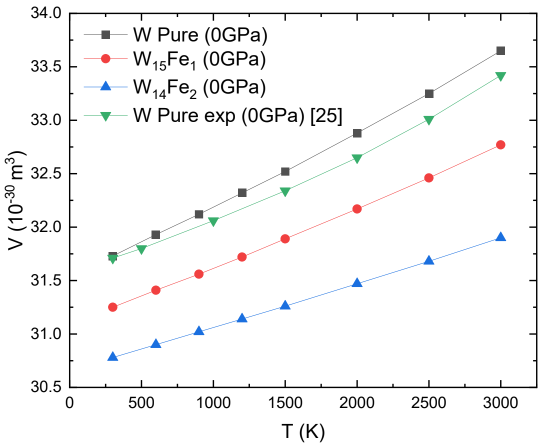

Figure 4. Temperature dependence of the volume for W and W–Fe alloys.

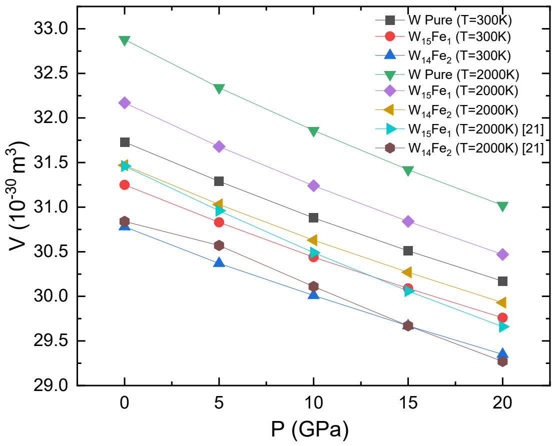

Figure 5. Pressure dependence of the atomic volume for W and W–Fe alloys at 300 K and 2000 K.

Figure 5 shows the plot of the change in atomic volume as a function of pressure from 0 to 20 GPa for W metal and the alloys $W_{15}Fe_1$ and $W_{14}Fe_2$ at two temperature levels: 300 K and 2000 K. The atomic volume decreases with increasing pressure, which reflects the crystal compression phenomenon under pressure - a well-known physical law. For the same material, the curve at 2000 K is always higher than the curve at 300 K, due to thermal expansion increasing the atomic volume. However, the rate of volume decrease with pressure does not change significantly, indicating that the materials maintain their structural stability even at high temperatures. Among the materials studied, $W_{14}Fe_2$ exhibits the smallest volume and the least decrease with pressure, suggesting better resistance to compression due to a denser lattice structure resulting from its higher Fe content. Pure W metal has the largest volume but is more easily compressed, while $W_{15}Fe_1$ shows intermediate properties between the two. The calculated results for the pressure dependence of the atomic volume are compared with the calculations by M. Zhang et al., [21] and show good agreement.

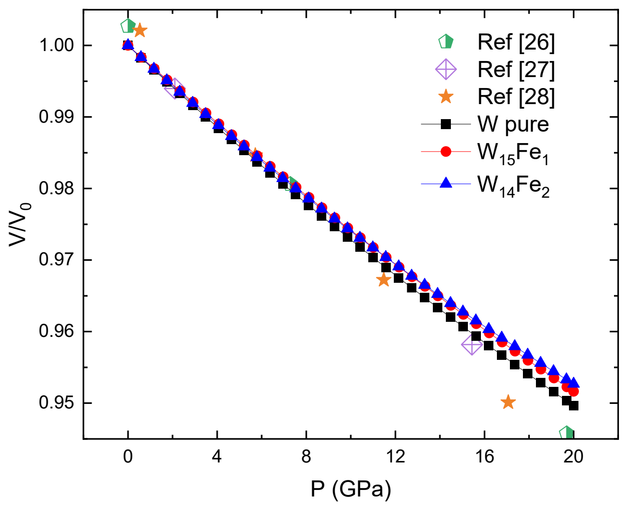

Figure 6. Pressure dependence of the atomic volume ratio for W and W–Fe alloys at 300 K.

The effect of pressure on the volume ratio V/V_o of W metal and $W_{15}Fe_1$, $W_{14}Fe_2$ alloys is shown in Figure 6. As the pressure increases, the V/V_o ratio of all three systems decreases almost linearly, indicating volumetric compression following the usual law for metallic materials. In the low-pressure region ($P < 10$ GPa), the difference between W and the Fe-containing alloys is almost insignificant. However, as the pressure increases to about 20 GPa, the $W_{14}Fe_2$ alloy shows a slightly larger V/V_o value compared to W and $W_{15}Fe_1$, suggesting that the Fe element slightly increases the compressibility of the crystal lattice. These calculated results show a tendency to agree well with the reference data [26- 28], demonstrating the high reliability of the simulation model.

3. Conclusions

In this study, we employed the Statistical Moment Method (SMM) and the Mie–Lennard-Jones pair interaction potential to derive analytical expressions and investigate the effects of temperature and pressure on the structural properties of tungsten (W) and W–Fe alloys. The results indicate that the lattice constant and atomic volume of all systems increase with temperature and decrease with pressure, consistent with the physical principles of thermal expansion and crystal compression. Substitution of Fe atoms into the W lattice reduces both the lattice constant and atomic volume, with the $W_{14}Fe_2$ alloy exhibiting the highest structural stability among the three examined samples. Comparison with experimental data and DFT calculations from the literature shows high reliability of the results, demonstrating the effectiveness of the SMM in simulating alloy systems under extreme conditions. This study contributes to clarifying the role of Fe in influencing the crystal structure and thermodynamic properties of the W–Fe system, providing a foundation for the design and optimization of materials for applications in energy, fusion, and high-temperature technologies.

References

[1] H. Bolt et al., Materials for the Plasma-facing Components of Fusion Reactors, Journal of Nuclear Materials, Vols. 329-333, Part A, 2004, pp. 66-73.

[2] R. Neu et al., Tungsten As First Wall Material in ASDEX Upgrade, Physica Scripta, Vol. T138, 2009, pp. 014038.

[3] Y. Mutoh, K. Ichikawa, K. Nagata et al., Effect of Rhenium Addition on Fracture Toughness of Tungsten at Elevated Temperatures, J. Mater. Sci., Vol. 30, 1995, pp. 770-775.

[4] D. Y. Jiang, W. B. Xiao, D. S. Liu, S. Q. Liu, Structural Stability, Electronic Structures, Mechanical Properties and Debye Temperature of W–Re Alloys: A First-Principles Study, Fusion Eng. Des., Vol. 162, 2021, pp. 112081.

[5] D. Y. Jiang, C. Y. Ouyang, S. Q. Liu, Mechanical Properties of W–Ti Alloys from First-Principles Calculations, Fusion Eng. Des., Vol. 106, 2016, pp. 34-39.

[6] G. A. Dosovitskiy, S. V. Samoilenkov, Thermal Expansion of Ni–W, Ni–Cr, and Ni–Cr–W Alloys Between Room Temperature And 800 °C, Int. J. Thermophys., Vol. 30, No. 6, 2009, pp. 1931-1937.

[7] B. X. Liu, L. J. Huang, L. Geng, Fabrication and Superior Ductility of Laminated Ti–Tibw/Ti Composites by Diffusion Welding, J. Alloys Compd., Vol. 602, 2014, pp. 187-192.

[8] Y. D. Kim, N. L. Oh, S. T. Oh, I. H. Moon, Thermal Conductivity of W–Cu Composites at Various Temperatures, Mater. Lett., Vol. 51, No. 5, 2001, pp. 420-424,

[9] F. Klein, A. Litnovsky, X. Y. Tan, J. G. Julian, M. Rasinski, C. Linsmeier, M. Bram, J. W. Coenen, Smart Alloys as Armor Material for DEMO: Overview of Properties and Joining to Structural Materials, Fusion Eng. Des., Vol. 166, 2021, pp. 112272.

[10] D. Y. Jiang, W. Hu, W. B. Xiao, H. Q. Wan, K. R. He, S. Q. Liu, Structural, Electronic, Mechanical and Thermodynamic Properties of Antiperovskites Ti_3Inx (X = C and N) Ceramics: a First-Principles Study, Vacuum, Vol. 204, 2022, pp. 111340.

[11] S. Biswas, First-Principles Investigation of the Metal–Insulator Transitions in Ti-Substituted Tetragonal Rutile VO_2, Vacuum, Vol. 212, 2023, pp. 111994.

[12] Y. Zhuang, Z. Y. Zou, B. Lu, Y. J. Li, D. Wang, M. Avdeev, S. Q. Shi, Understanding the Li Diffusion Mechanism and Positive Effect of Current Collector Volume Expansion in Anode-Free Batteries, Chin. Phys. B, Vol. 29, 2020, pp. 068202.

[13] N. Tang, V. V. Hung, Investigation of the Thermodynamic Properties of Anharmonic Crystals by Momentum Method. I. General Results for Face-Centred Cubic Crystals, Phys. Status Solidi B, Vol. 149, No. 2, 1988, pp. 511-519, https//doi.org/10.1002/Pssb.2221490212.

[14] K. M. Jindo, S. R. Nishitani, V. V. Hung, Hcp–Bcc Structural Phase Transformation of Titanium: Analytic Model Calculations, Phys. Rev. B, Vol. 70, No. 18, 2004, pp. 184122, https//doi.org/10.1103/Physrevb.70.184122.

[15] V. V. Hung, N. T. Hai, Investigation of the Elastic Moduli of Face- and Body-Centered Cubic Crystals, Comput. Mater. Sci., Vol. 14, 1999, pp. 261-266, https//doi.org/10.1016/S0927-0256(98)00117-7.

[16] T. D. Cuong, N. Q. Hoc, A. D. Phan, N. T. Thao, N. D. Trung, Theoretical Predictions of Melting Behaviors of Hcp Iron up to 4000 Gpa, Phys. Rev. B, Vol. 106, No. 9, 2022, pp. 094103, https//doi.org/10.1103/Physrevb.106.094103.

[17] C. H. Phuong, V. V. Hung, Influence of Temperature and Pressure on the Lattice Constant of $Srtio_3$ Perovskite by the Statistical Moment Method with Improved Interatomic Potential, Math. Phys., Vol. 38, No. 3, 2022, https//doi.org/10.25073/2588-1124/Vnumap.4706.

[18] N. Q. Hoc, T. T. Nga, N. N. Thang, B. L. Ngoc, N. T. Ngoc, L. T. Lam, Toward Better Understanding of Anharmonic Structural, Thermodynamic, and Elastic Properties of Casio3_33 Perovskite Under Extreme Conditions Via Statistical Moment Method, Materialia, Vol. 34, 2024, pp. 102105, https//doi.org/ 10.1016/J.Mtla.2024.102105.

[19] S. Baty, L. Burakovsky, D. Preston, Topological Equivalence of the Phase Diagrams of Molybdenum and Tungsten, Crystals, Vol. 10, No. 1, 2020, pp. 20, https//doi.org/10.3390/Cryst10010020.

[20] E. Y. Tonkov, E. G. Ponyatovsky, Phase Transformations of Elements Under High Pressure. Boca Raton, FL: CRC Press, 2004, pp. 253-265.

[21] M. Zhang, X. Wang, Y. Chen, H. Cai, H. Li, D. Jiang, Theoretical Study of Mechanical and Thermodynamic Properties of W–Fe Alloys: Promising Ultra-High Temperature Alloy Materials, Vacuum, Vol. 222, 2024, pp. 113047, https//doi.org/10.1016/J.Vacuum.2024.113047.

[22] N. Tang, V. V. Hung, Investigation of the Thermodynamic Properties of Anharmonic Crystals by Momentum Method. IV, The Limiting of Absolute Stabi0, lity and the Melting Temperature of Crystals, Phys. Status Solidi B, Vol. 162, No. 2, 199, pp. 379-385, https//doi.org/oi: 10.1002/Pssb.2221620207.

[23] M. N. Magomedov, The Calculation of the Parameters of the Mie–Lennard-Jones Potential, High Temp., Vol. 44, No. 4, 2006, pp. 513-529, https//doi.org/10.1134/S0018151X06040099.

[24] K. D. Litasov, P. N. Gavryushkin, P. I. Dorogokupets, I. S. Sharygin, A. Shatskiy, Y. Fei, S. V. Rashchenko, Y. V. Seryotkin, Y. Higo, K. Funakoshi, E. Ohtani, Thermal Equation of State to 33.5 Gpa and 1673 K and Thermodynamic Properties of Tungsten, J. Appl. Phys., Vol. 113, 2013, pp. 133505.

[25] D. Y. Jiang, Q. Zhou, L. Xue, T. Wang, J. F. Hu, First-Principles Study of the Phase Stability and Mechanical Properties of Binary W–Mo Alloys, Fusion Eng. Des., Vol. 130, 2018, pp. 56-61.

[26] K. D. Litasov, P. N. Gavryushkin, P. I. Dorogokupets, I. S. Sharygin, A. Shatskiy, Y. Fei, S. V. Rashchenko, Y. V. Seryotkin, Y. Higo, K. Funakoshi, E. Ohtani, Thermal Equation of State to 33.5 Gpa and 1673 K and Thermodynamic Properties of Tungsten, J. Appl. Phys., Vol. 113, 2013, pp. 133505.

[27] Y. Wang, D. Chen, X. Zhang, Phonon Softening and Phase Transitions in Metals Under Pressure, Phys. Rev. Lett., Vol. 84, 2000, pp. 3220.

[28] S. Xiang, F. Xi, Y. Bi, J. A. Xu, H. Geng, L. Cai, F. Jing, J. Liu, Elastic and Thermodynamic Properties of Bcc Tungsten Under High Pressure, Phys. Rev. B, Vol. 81, 2010. pp. 014301.